SCIENCE CHINA Information Sciences



RESEARCH PAPER

March 2026, Vol. 69, Iss. 3, 132301:1–132301:15 https://doi.org/10.1007/s11432-025-4551-x

Communication, sensing and control integrated closed-loop system: modeling, control design and resource allocation

Zeyang MENG, Dingyou MA, Zhiqing WEI, Ying ZHOU & Zhiyong FENG*

Key Laboratory of Universal Wireless Communications, Beijing University of Posts and Telecommunications, Beijing 100876, China

Received 19 March 2025/Revised 3 July 2025/Accepted 12 August 2025/Published online 28 October 2025

Abstract The wireless communication technologies have fundamentally revolutionized industrial operations. The operation of the automated equipment is conducted in a closed-loop manner, where the status of devices is collected and sent to the control center through the uplink channel, and the control center sends the calculated control commands back to the devices via downlink communication. However, existing studies neglect the interdependent relationship between uplink and downlink communications, and there is an absence of a unified approach to model the communication, sensing, and control within the loop. This can lead to inaccurate performance assessments, ultimately hindering the ability to provide guidance for the design of practical systems. Therefore, this paper introduces an integrated closed-loop model that encompasses sensing, communication, and control functionalities, while addressing the coupling effects between uplink and downlink communications. Through the analysis of system convergence, an inequality pertaining to the performances of sensing, communication, and control is derived. Additionally, a joint optimization algorithm for control and resource allocation is proposed. Simulation results are presented to offer an intuitive understanding of the impact of system parameters. The findings of this paper unveil the intricate correlation among sensing, communication, and control, providing insights for the optimal design of industrial closed-loop systems.

 $\textbf{Keywords} \quad \text{closed-loop system, wireless network, effective-capacity, model predictive control}$

Citation Meng Z Y, Ma D Y, Wei Z Q, et al. Communication, sensing and control integrated closed-loop system: modeling, control design and resource allocation. Sci China Inf Sci, 2026, 69(3): 132301, https://doi.org/10.1007/s11432-025-4551-x

1 Introduction

Recently, the rapid progress of wireless communication technologies, particularly 5G and the forthcoming 6G, has initiated a fundamental change in industrial settings [1,2]. The wireless network liberates automated equipment from the constraints of cables, ensuring mobility for devices such as the mobile robotic arm and automated guided vehicle (AGV). This advancement enables manufacturers to flexibly alter the structure of the production line and adjust manufacturing processes based on the order demands, thereby enhancing the production efficiency and reducing manufacturing costs [3,4].

The operational process of automated equipment with the wireless network is based on the iterative closed-loop process, as shown in Figure 1.

Specifically, sensors collect the status information of equipment, which is then transmitted to the control center via uplink wireless channels. The control center generates the control commands based on the sensed data and then sends these commands back to the controlled equipment through downlink wireless communication. In such a process, the performance of communication, sensing, and control is closely interrelated. Sensing affects not only the accuracy of control commands but also the data load in the communication process. In addition, the communication capability of the system determines whether the control center can receive fresh sensing information in a timely manner.

These intricate mutual dependencies demonstrate that, in practical industrial closed-loop systems, communication, sensing, and control are inherently and tightly coupled [5]. Treating them as independent components leads to several significant drawbacks. Specifically, a separate design may result in sub-optimal system performance and significant deviations between theoretical analysis and real-world outcomes, as the intricate cross-layer interactions and trade-offs, such as the impact of communication delays or sensing accuracy on control stability, cannot be fully captured or balanced. Such neglect often leads to inefficient resource allocation, unnecessary energy or bandwidth

^{*} Corresponding author (email: fengzy@bupt.edu.cn)

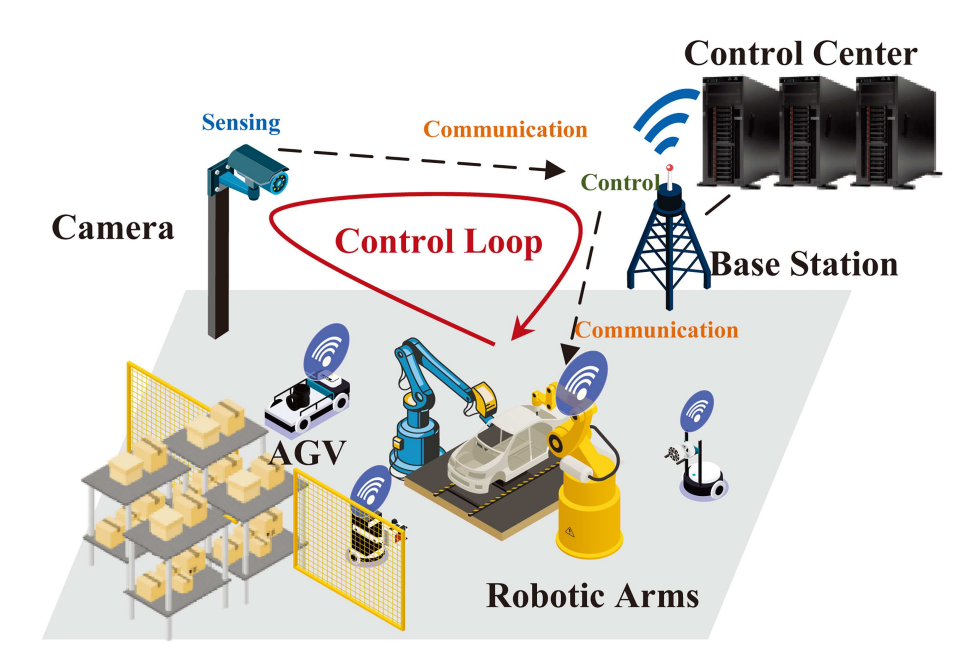


Figure 1 (Color online) A typical closed-loop process in the typical industry with a wireless network.

consumption, and reduced robustness, since errors or delays in one subsystem may propagate and amplify throughout the closed-loop system. Moreover, independent treatment of these elements makes it virtually impossible to quantitatively model or optimize the trade-offs between key system-level objectives, such as delay, stability, and resource utilization.

Consequently, a unified consideration of communication, sensing, and control is fundamentally required to achieve optimal system performance. Nevertheless, the joint consideration of communication, sensing, and control also introduces considerable research challenges. The primary difficulty lies in the fact that parameters across these domains are highly coupled and interact in complex, often nonlinear, ways, making it extremely challenging to construct unified and tractable mathematical models. Quantifying the relationship between high-level performance metrics (such as delay and stability) and underlying system parameters (such as bandwidth allocation and convergence rate) are particularly difficult, yet necessary for practical design and optimization. Furthermore, the resulting cross-domain optimization problems are typically non-convex and involve multiple objectives and constraints, which significantly increases their complexity. As a result, existing studies have explored different strategies for modeling and optimizing these systems, which can be broadly classified into two kinds of approaches: control-centric and communication-centric.

Control-centric approaches are generally based on the dynamic equations of devices under simple conditions. Specifically, communication performance is simplified as predefined constants [6–8] or bounded random variables [9,10], and is then integrated into dynamic equations. Sensing performance, including quantization errors [11] and estimation errors [12], is also taken into consideration in some research. Subsequently, the stability of the system is analyzed, and new robust control methods are proposed based on the new dynamic equations. The limitation of this approach lies in the disparity between theoretical communication models and real-world communication systems. This gap hinders the achievement of expected control effects and poses challenges in the design of communication systems. In addition, there is a lack of unified modeling of interactions among communication, sensing, and control.

Communication-centric approaches employ parameters such as linear quadratic regulator (LQR) cost [13, 14] and convergence rate [15, 16] to model the efficiency of control systems. These parameters are integrated with the metrics of communication performance, such as mutual information [13, 14] and channel capacity [17–20], to establish a unified performance index or to derive an optimal design for the communication system. The limitation of this approach is that the uplink and downlink communications are modeled independently, which contradicts the characteristic of control loops where the data carried by the downlink are closely related to the uplink sensing data. Additionally, preset control parameters make it difficult for the system to achieve globally optimal control effects. Furthermore, few studies consider the impact of sensing errors on system performance, which may lead to deviations in performance when communication designs are applied in practical systems.

To address the above shortcomings, we establish a sensing-communication-control integrated closed-loop model to address the aforementioned shortcomings, and propose a joint optimization method for control and resource allo-

cation. Specifically, to address the issue of the separation between uplink and downlink models of communication-centric approaches, we develop an uplink-downlink coupled communication model based on the effective capacity theory, which establishes a correlation between the network performance and communication resources. On this basis, closed-form expressions for closed-loop delay and packet loss rate are derived to quantitatively describe the key communication indicators that influence control performances, thereby resolving the problem of over-simplified communication metrics in control-centric approaches.

Furthermore, in order to describe the interaction of communication, sensing, and control processes, we develop a control model that accounts for delay, packet loss, and estimation error. Additionally, we formulate a sensing-estimation model to derive the boundary of the estimation error. To clarify the complex relationship among communication, sensing, and control parameters, an inequality involving convergence rate, bandwidth, and quantization level is derived by applying Lyapunov stability theory [21] based on the proposed model.

Finally, to provide guidance for both communication and control within the closed-loop system, a joint optimization problem for control and resource allocation is proposed, which is highly non-convex. To address this optimization challenge, a differential evolution (DE)-based optimization algorithm [22] is employed to acquire global optimum solutions. The simulation demonstrates the nonlinear effect of parameters such as closed-loop delay, convergence rate, and quantization level, whose excessively high or low values will adversely impact the accomplishment of control tasks due to the coupling relationship among communication, sensing, and control. These phenomena have not yet been explored in existing research.

The main contributions are summarized as follows.

- Based on the effective capacity theory, a joint modeling of the uplink and downlink communication processes is conducted. From this model, closed-form expressions for closed-loop delay and packet loss rate are derived, establishing a relationship between the closed-loop performance and network resources.
- An inequality for the system convergence rate is derived by incorporating the effects of three aspects: sensing, communication, and control, which characterizes the complex constraining relationship among these three functionalities.
- A joint optimization algorithm is proposed, achieving efficient utilization of communication resources while ensuring control effectiveness. The global optimal solution for this problem is obtained based on a heuristic method.

The rest of this article is organized as follows. In Section 2, the system model of the wireless closed-loop control system is established, which provides the main analytical results of this article. In Section 3, the joint optimization of sensing, control, and communication is carried out, where a heuristic method is applied to solve the non-convex problem. In Section 4, simulation results are provided for both the result of the optimization problem and the control strategy proposed in the system model. Finally, concluding remarks are provided in Section 5 and the potential research directions for the future work are provided in Section 6.

2 System model

The system model of a wireless closed-loop system is shown in Figure 2, which is composed of the actuator, the digital sensor, two wireless channels, and a control center [23–25]. The closed-loop process starts from the digital sensor, which perceives the state information of the actuator and quantifies it into quantized values. These quantized states are then transmitted to the control center through the wireless uplink channel, and processed to acquire the estimated state to recover the state of the actuator. Subsequently, the controller at the control center generates control commands with the estimated state and transmits them to the actuator through the wireless downlink channel. The commands are then executed on the actuator, so that the closed-loop process is completed. In the sequel, the system model is introduced separately from the perspectives of communication, control, and sensing. The coupling inequality among the performances of these three functions is derived from the viewpoint of system convergence.

2.1 Communication model

In a closed-loop system, the wireless communication primarily handles the uploading of sensing data and the dispatching of control instructions. Therefore, a closed-loop communication model is constructed in this section with uplink-downlink tandem queues. The performance of the communication system is measured by two typical indicators, i.e., the closed-loop delay D_c and the packet loss rate ϵ_c . The closed-loop delay D_c represents the total time from the transmission of sensing packets to the reception of the corresponding control instructions. Excessive closed-loop delay can lead to imprecise control instructions, thereby affecting the control effectiveness. Besides, the

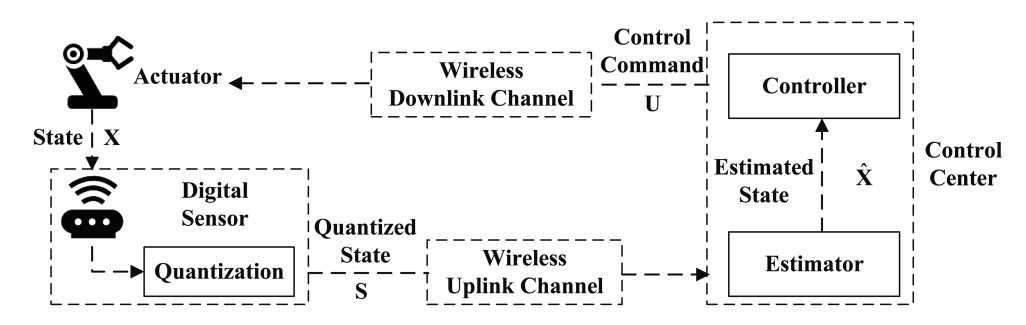


Figure 2 System model of a wireless closed-loop control system.

packet loss rate ϵ_c reflects the probability of data packets being discarded due to factors such as timeouts during the entire communication process, which results in reduced system robustness and lower convergence ability.

In the following analysis, we first establish a model of a single queue. The closed-form expression for the effective capacity of a single queue under Rayleigh fading channels, as well as the limitations of the arrival rate, is derived. On the basis of these results, the properties of the closed-loop delay, the packet loss rate, and the maximum arrival rate in tandem queues are derived, and the closed-form results are presented to better assist in system design.

2.1.1 Single queue effective capacity model

The derivation of this part is based on the following assumptions.

Assumption 1. The arrival of data packets in the uplink queue is periodic and the size of each packet is the same.

Assumption 2. The size of the control data packets is consistent, and the amount of sensing data required to generate each control command is fixed.

Assumption 3. The channel fading follows a Rayleigh distribution. Besides, effects such as frequency-selective fading, multi-path propagation, and Doppler shift are not considered.

Assumption 1 holds because the packets in the uplink queue originate from sensors, which usually sense periodically in the factory, and the format of these packets is typically consistent¹⁾. Assumption 2 is determined by the control algorithm. Since the control algorithm often remains unchanged in each iteration, it is reasonable to consider Assumption 2 as valid. Assumption 3 is reasonable because, in factories, there are often many obstructions and scatters, with rare direct paths [26,27]²⁾. Besides, AGVs and similar industrial devices typically operate at low speeds in factory environments [1].

Under the above assumptions, the number of arrivals data per second, i.e., the arrival rate, of the uplink queue λ_u is constant according to Assumption 1. Besides, according to Assumption 2, the arrival rate of the downlink queue, denoted by λ_d , has a linear relationship with the amount of data departing from the uplink queue per second, i.e., the uplink departure rate L_u , which is

$$\lambda_d = c_d L_u. \tag{1}$$

In this work, c_d is treated as a constant, which implicitly assumes that each downlink control packet has a fixed size and structure. This reflects the scenario where each unit of uplink data generates a consistent amount of downlink control information. We acknowledge that, in practice, dynamic adjustment of downlink packet size could be realized, for example, by reducing the resolution of control commands or simplifying their structure when network resources are limited. However, for the sake of clarity and consistency in analysis, and to focus on the core closed-loop relationship between uplink sensing and downlink control, we maintain the fixed packet size assumption in our model.

Besides, the service rate of the queue denotes the average number of items that can be served by the queue per unit of time. In the proposed communication model, the service rate is the average number of packages transmitted

¹⁾ Assumption 1 is consistent with typical industrial scenarios and standards such as 3GPP TS 22.261 [1], where most sensors perform periodic sampling and reporting. In practice, there may be occasional cases where the reporting interval of a sensor changes due to manual reconfiguration or specific application requirements. As long as the reporting interval remains fixed for a certain period, the periodic arrival assumption and the corresponding analysis remain valid within that period. For scenarios involving event-triggered or highly adaptive sensing, where the arrival process is fundamentally non-periodic, a different modeling approach would be required. These scenarios are not the focus of this work

²⁾ This assumption is widely adopted for industrial environments with rich scattering and non-line-of-sight (NLOS) propagation, where direct paths are rare due to obstacles such as metallic equipment [26, 27]. More complex models can also be integrated into our analytical framework by adapting the expectation in Theorem 1, at the cost of tractability.

per second, i.e., the transmission rate of the communication channel. Therefore, according to Assumption 3, the service rate of two queues, i.e., the capacity of uplink and downlink channels R_u and R_d satisfies

$$R_i = W_i \log_2(1 + \text{SNR}_i \cdot \gamma_i^2), i = u, d, \tag{2}$$

where SNR_i is the constant number of signal-to-noise ratio (SNR) obtained by dividing the expectation of the signal power by the expectation of the noise power, and W_i is the bandwidth of the uplink and downlink channels. Parameter γ is the fading coefficient, which is a random variable following the Rayleigh distribution. Therefore, γ^2 follows the exponential distribution [28]. It should be noted that in practical industrial environments, the channel fading process may exhibit temporal correlation. Our framework can accommodate such cases by substituting the effective capacity under correlated fading channels, but the closed-form expressions are generally unavailable, and numerical evaluation is required. The Rayleigh assumption thus strikes a balance between analytical tractability and practical relevance.

Subsequently, the effective capacity theory is employed to connect the link-layer performance with physical layer resources. The application of the effective capacity theory is motivated by the characteristics of industrial closed-loop systems, where traffic is typically periodic and deterministic, dictated by fixed sampling and actuation cycles as required by industrial standards. Moreover, the effective capacity framework enables a direct and explicit relationship between link-layer performance metrics (such as delay and packet loss) and underlying physical-layer parameters (including bandwidth, SNR, and channel fading), which is particularly valuable for cross-layer analysis and practical resource allocation in wireless industrial applications. The effective capacity is defined as the maximum acceptable amount of bits that the channel can handle per unit of time, which is given by [29],

$$C_i(\theta_i, R_i) = -\frac{1}{\theta_i} \ln \left(\mathbb{E} \{ \exp(-\theta_i R_i) \} \right), i = u, d,$$
(3)

where C_u and C_d are effective capacities of the uplink and downlink communications, respectively. The parameter θ_i represents the decay rate of the queue overflow probability, which satisfies

$$\lim_{q_{i,0}\to\infty} \frac{\ln \Pr\{q_i(\infty)\geqslant q_{i,0}\}}{q_{i,0}} = -\theta_i, i = u, d,$$
(4)

with $q_i(\infty)$ being the length of the communication buffer queue in steady state, and $q_{i,0}$ being the buffer overflow threshold.

With Assumption 3, the effective capacities of the uplink and downlink queues follow Theorem 1.

Theorem 1 (Effective capacity of Rayleigh channel). The effective capacity of uplink and downlink queues under Assumption 3 is approximated by

$$C_i(\theta_i, W_i, \text{SNR}_i, \beta_i) = \frac{1}{\theta_i} \ln(\text{SNR}_i \beta_i) \left(\frac{W_i \theta_i}{\ln 2} - 1 \right) - \frac{1}{\text{SNR}_i \beta_i}, \quad i = u, d,$$
 (5)

where β_i is the rate parameter of the random variable γ^2 in the uplink and downlink channels.

Proof. See the proof in Appendix A.

According to the definition of the effective capacity, C_i is the maximum data volume that the queue can accommodate. Therefore, it should satisfy the following inequalities:

$$\lambda_i \leqslant C_i(\theta_i, W_i, \text{SNR}_i, \beta_i) = \frac{1}{\theta_i} \ln(\text{SNR}_i \beta_i) \left(\frac{W_i \theta_i}{\ln 2} - 1 \right) - \frac{1}{\text{SNR}_i \beta_i}, \quad i = u, d.$$
 (6)

Moreover, packets are considered to be lost when their delay exceeds a specified threshold. Consequently, the packet loss rate, denoted by ϵ_i , is defined as

$$\epsilon_i = P(D_i > D_{i,\text{max}}) = e^{-D_{i,\text{max}}\theta_i C_i(\theta_i, W_i, \text{SNR}_i, \beta_i)},$$
(7)

where D_i is the delay of the packet, and $D_{i,\text{max}}$ is the threshold for packet loss [30, Eq. 3].

2.1.2 Analysis of the tandem queue

Based on the analysis of a single queue above, we further consider the performance metrics for the tandem queue of the close-loop communication.

We would like to further emphasize the inherent coupling between the uplink and downlink queues by noting that the uplink queue carries the sensing data collected by sensors from the controlled device, which, after being processed by the controller, is used to generate control instructions that are transmitted via the downlink. This mechanism leads to a situation where changes in the uplink queue's traffic, such as increases in arrival rate or improvements in channel capacity, will directly impact the load on the downlink queue, thereby requiring additional resources on the downlink side to maintain system stability. At the same time, the queuing and service parameters of both uplink and downlink, including bandwidth allocation and effective channel capacity, jointly determine the overall closed-loop delay D_c and packet loss rate ϵ_c . Therefore, under constraints on delay and reliability, any degradation in one link's communication performance will necessitate compensatory resource allocation in the other to meet the overall system requirements. With these coupling effects in mind, we now proceed to derive the closed-form expressions for the closed-loop delay, packet loss rate, and maximum arrival rate for the tandem queue model.

The closed-form expressions of the closed-loop delay D_c , the packet loss rate ϵ_c , and the maximum arrival rate λ_{max} are given in the following theorems.

Theorem 2 (Packet loss rate and closed-loop delay). Considering that $D_{c,\text{max}}$ is the threshold of the closed-loop delay D_c that leads to packet loss, the packet loss rate ϵ_c is given by

$$\epsilon_c = \frac{e^{-D_{c,\max}\mu_d}\mu_u - e^{-D_{c,\max}\mu_u}\mu_d}{\mu_u - \mu_d}.$$
 (8)

The exception of the closed-loop delay is derived as

$$E\left[D_{c}|D_{c} < D_{c,\max}\right] = \left[\mu_{u}^{2} - \mu_{d}^{2} + e^{-D_{c,\max}\mu_{u}}\mu_{d}^{2}\left(1 + D_{c,\max}\mu_{u}\right) - e^{-D_{c,\max}x\mu_{d}}\mu_{u}^{2}\left(1 + D_{c,\max}\mu_{d}\right)\right]/\mu_{u}\mu_{d}\left(\mu_{u} - \mu_{d} + e^{-D_{c,\max}x\mu_{u}}\mu_{d} - e^{-D_{c,\max}\mu_{d}}\mu_{u}\right),$$

$$(9)$$

where

$$\mu_i = \ln(\mathrm{SNR}_i \beta_i) \left(\frac{W_i \theta_i}{\ln 2} - 1 \right) - \frac{\theta_i}{\mathrm{SNR}_i \beta_i}, \quad i = u, d.$$
 (10)

Proof. See the proof in Appendix B.

Theorem 3 (Maximum arrival rate). When $\theta_u > \theta_d$, the maximum arrival rate λ_{max} satisfies

$$\lambda_{\max} = \min \left\{ \frac{1}{\theta_u} \ln(SNR_u \beta_u) \left(\frac{W_u \theta_u}{\ln 2} - 1 \right) - \frac{1}{SNR_u \beta_u}, \frac{1}{c_d \theta_d} \ln(SNR_d \beta_d) \left(\frac{W_d \theta_d}{\ln 2} - 1 \right) - \frac{1}{SNR_d \beta_d} \right\}. \tag{11}$$

Besides, when $\theta_u < \theta_d$,

$$\lambda_{\max} = \min \left\{ \frac{1}{\theta_u} \ln(SNR_u \beta_u) \left(\frac{W_u \theta_u}{\ln 2} - 1 \right) - \frac{1}{SNR_u \beta_u}, \\ \frac{1}{c_d \theta_u} \ln \left[\left(SNR_d \beta_d \right) \left(\frac{W_d \theta_d}{\ln 2} \right) \left(SNR_u \beta_u \right)^{c_d} \left(\frac{W_u \left(\theta_d - \theta_u \right)}{\ln 2} \right)^{c_d} \right] \right\}.$$
 (12)

Proof. See the proof in Appendix C.

2.2 Control model

The control system serves as the backbone of a closed-loop system. The purpose of the control stage is to generate the control commands based on the current state of the device, so as to enable the device to reach the expected state after a period of time. In the field of control, dynamic functions are often applied to model the state evolution. The following subsections progressively establish the dynamic function of the closed-loop system, advancing from a simple model to a model with imperfect sensing, and finally to a model influenced by imperfect wireless communication.

$2.2.1 \quad Basic\ control\ model$

The model starts from a basic state-space control model [31], i.e.,

$$\dot{\mathbf{X}} = \mathbf{A}\mathbf{X} + \mathbf{B}\mathbf{U},\tag{13}$$

where $\mathbf{X} = \{x_1, x_2, \dots, x_n\}$ is the state vector of the actuator with n states, \mathbf{U} is the control vector, which is determined by the control command. \mathbf{A} and \mathbf{B} are system matrices which are guaranteed by physical characteristics

of the system. The state evolution of nearly all devices can be represented in this form, such as AGVs [32] and robotic arms [33].

For example, for the movement control of AGVs [32], $\mathbf{X} = [\delta, v, a]^{\mathrm{T}}$, with δ, v , and a being the position, velocity, and acceleration, respectively. \mathbf{U} is a linear control strategy, which is the linear combination of the state \mathbf{X} . With such control strategy, \mathbf{A} and \mathbf{B} are given by

$$\mathbf{A} = \begin{bmatrix} 0 & 1 & 0 \\ 0 & 0 & 1 \\ 0 & 0 & -1/\varsigma \end{bmatrix}, \quad \mathbf{B} = \begin{bmatrix} 0, 0, -1/\varsigma \end{bmatrix}^{\mathrm{T}}, \tag{14}$$

respectively, where ς is a constant related to the engine.

For ease of analysis, Eq. (13) can be discretized with Euler's method [34].

Specifically, expand the continuous-time solution as a Taylor series at each step as

$$\mathbf{X}_{t+1} = \mathbf{X}_t + T_d \dot{\mathbf{X}} + \frac{T_d^2}{2} \ddot{\mathbf{X}} + \cdots$$
 (15)

with \mathbf{X}_t being the state of time t, and T_d being the time interval where the device is assumed to be constant. By retaining only the first-order term and neglecting higher-order terms, the discrete-time approximation becomes

$$\dot{\mathbf{X}} \approx \frac{1}{T_d} (\mathbf{X}_{t+1} - \mathbf{X}_t). \tag{16}$$

Substituting (16) into (13), the control model at time t is expressed as

$$\frac{1}{T_d}(\mathbf{X}_{t+1} - \mathbf{X}_t) = \mathbf{A}\mathbf{X}_t + \mathbf{B}\mathbf{U}_t. \tag{17}$$

Suppose a linear control strategy is applied, i.e., $\mathbf{U} = \mathbf{K}\mathbf{X}$ with $\mathbf{K} = [K_1, K_2, K_3]$, which is widely applied in [35–37]. The control model (17) can be reorganized as

$$\mathbf{X}_{t+1} = \widetilde{\mathbf{A}} \mathbf{X}_t + \widetilde{\mathbf{B}} \mathbf{K} \mathbf{X}_t, \tag{18}$$

where $\widetilde{\mathbf{A}} = T_d \mathbf{A} + \mathbf{I}$ and $\widetilde{\mathbf{B}} = T_d \mathbf{B}$.

2.2.2 Control model considering imperfect sensing and wireless communication

The imperfect sensing, followed by the subsequent estimation process, complicates the controller's task of generating control commands. These commands depend on accurate state information of the actuator, and any inaccuracies in this process can lead to control deviation. To model the impact of the imperfect sensing and estimation on the dynamic function, let $\hat{\mathbf{X}}_t$ denote the estimate of the state \mathbf{X} . The device then receives the estimated-state-based control command $\hat{\mathbf{U}}_t = \mathbf{K}\hat{\mathbf{X}}_t$, rather than the actual-state-based command $\mathbf{U}_t = \mathbf{K}\mathbf{X}_t$. Therefore, Eq. (18) can be developed as

$$\mathbf{X}_{t+1} = \widetilde{\mathbf{A}} \mathbf{X}_t + \widetilde{\mathbf{B}} \mathbf{K} \hat{\mathbf{X}}_t. \tag{19}$$

The effect of wireless communication can be attributed to the inaccurate control caused by communication delay and the loss of control instructions due to the package loss. When the communication delay occurs, the device will receive control commands corresponding to the previous state rather than the current state, resulting in a suboptimal control strategy. However, the delay-compensated strategy can be applied to compensate for the impact of communication delay [7,38]. Therefore, a delay-compensation control method is proposed, as Figure 3.

Based on the control objective, the control center generates the optimal linear control law coefficient **K** in advance. After the current device's state is uploaded to the control center at time t_0 , the estimated state $\hat{\mathbf{X}}_{t_0}$ is obtained through estimation, and the states for the subsequent N time instants are subsequently estimated. Based on the estimated N state values, control sequences for the corresponding N time instants are generated. The sequence is transmitted to the device entirely, and appropriate data packets are selected based on the discretized time interval from the sending of perception data to the receiving of control packets, i.e., $\lfloor D_c/T_d \rfloor$, where $\lfloor \cdot \rfloor$ represents the floor function.

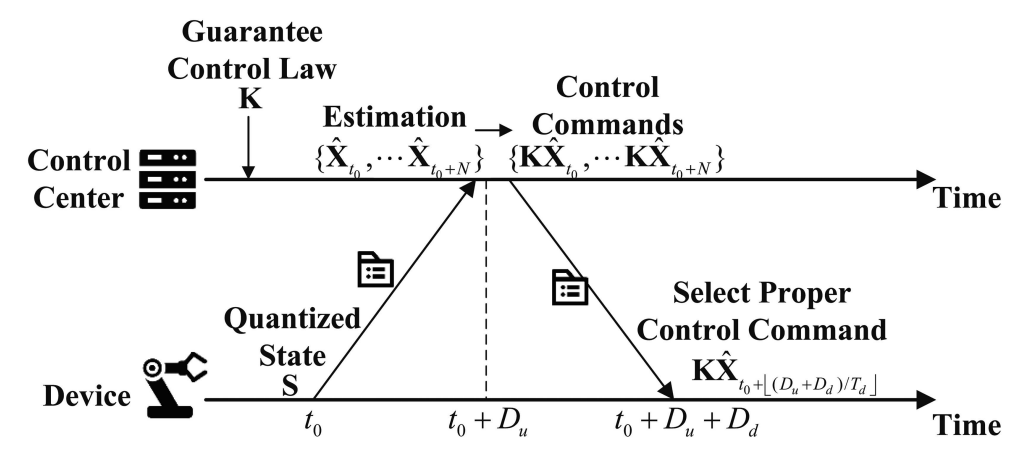


Figure 3 The delay-compensation control method.

Based on the above analysis, the impact of packet loss on the iteration of system states is further considered. When the packet loss occurs, the control command cannot be transmitted to the device, and the state equation relies on the physical properties during uncontrolled iterations, that is

$$\mathbf{X}_{t+1} = \widetilde{\mathbf{A}} \mathbf{X}_t + \eta \widetilde{\mathbf{B}} \mathbf{K} \hat{\mathbf{X}}_t, \tag{20}$$

where η is a random variable which equals 0 with probability ϵ_c and equals 1 with probability $1 - \epsilon_c$.

2.3 Sensing and estimation model

The sensing-estimation process is located in the first half of the closed-loop process. The sensor detects the current state of the actuator and quantifies it into a digital signal, which is then transmitted to the control center. At the control center, the future states are estimated according to the received information to compensate for the communication delays, which is introduced as the control model and Figure 3. In the subsequent analysis, a uniform quantization method is adopted. Further analysis is conducted on the errors introduced by the quantization and estimation.

Suppose the sensors are capable of locally acquiring the state information of the actuators with high accuracy; i.e., the data prior to quantization are accurate. Besides, the detection of the quantization is assumed to lie in the area of $[\mathbf{X}_L, \mathbf{X}_U]$. Let r denote the quantization level; i.e., the area $[\mathbf{X}_L, \mathbf{X}_U]$ is uniformly quantized into 2^r intervals. Hence, the sensing data generated per unit time, also known as the arrival rate of the uplink queue, can be represented as

$$\lambda_u = \frac{r}{T_d}.\tag{21}$$

Besides, the midpoint of the interval is taken as the quantization of X_t , which is denoted by X_t^q .

$$\mathbf{X}_t^q = \mathbf{X}_L + \left(j + \frac{1}{2}\right) \cdot \frac{1}{2^r} [\mathbf{X}_U - \mathbf{X}_L],\tag{22}$$

where $j \in \{0, 1, \dots, 2^r - 1\}$. Therefore, the quantization error for \mathbf{X}_t can be formulated as

$$\mathbf{e}_0 = \mathbf{X}_t^q - \mathbf{X}_t \in \left[\frac{1}{2} \frac{1}{2^r} [\mathbf{X}_L - \mathbf{X}_U], \frac{1}{2} \frac{1}{2^r} [\mathbf{X}_U - \mathbf{X}_L] \right]. \tag{23}$$

On the assumption that the error \mathbf{e}_0 follows the uniform distribution, which is a usual assumption in a generalized control system [23], we obtain

$$\mathbb{E}[\mathbf{e}_0] = \mathbb{E}[\mathbf{X}_t^q - \mathbf{X}_t] = 0, \tag{24}$$

$$\mathbb{E}[\mathbf{e}_0^{\mathrm{T}}\mathbf{e}_0] = \frac{1}{12} \frac{1}{A^T} [(\mathbf{X}_L - \mathbf{X}_U)^{\mathrm{T}} (\mathbf{X}_L - \mathbf{X}_U)]. \tag{25}$$

After quantization, the estimator at the controller should estimate the future N states for generating the control sequence to compensate the communication delay, where the estimation is made by

$$\hat{\mathbf{X}}_{t+1} = \widetilde{\mathbf{A}}\hat{\mathbf{X}}_t + \mathbb{E}(\eta)\widetilde{\mathbf{B}}\mathbf{K}\hat{\mathbf{X}}_t = \widetilde{\mathbf{A}}\hat{\mathbf{X}}_t + (1 - \epsilon_c)\widetilde{\mathbf{B}}\mathbf{K}\hat{\mathbf{X}}_t = \mathbf{A}_K\hat{\mathbf{X}}_t,$$
(26)

where $\mathbf{A}_K = \widetilde{\mathbf{A}} + (1 - \epsilon_c)\widetilde{\mathbf{B}}$. According to the iteration (26), the estimation of the future state at time $t + \tau$ is

$$\hat{\mathbf{X}}_{t+\tau} = (\mathbf{A}_K)^{\tau} \hat{\mathbf{X}}_t. \tag{27}$$

Therefore, the mean estimation error of time $t+\tau$ is obtained as

$$\mathbb{E}[\mathbf{e}_{\tau}] = \mathbb{E}[\hat{\mathbf{X}}_{t+\tau} - \mathbf{X}_{t+\tau}] = (\mathbf{A}_K)^{\tau} (\mathbf{X}_t^q - \mathbf{X}_t) = 0.$$
(28)

Besides, when $\text{Tr}(\widetilde{\mathbf{A}}^T\widetilde{\mathbf{A}}) \neq 1$, the mean square estimation error satisfies

$$\mathbb{E}[\mathbf{e}_{\tau}^{\mathrm{T}}\mathbf{e}_{\tau}] \leqslant \frac{1}{12} \frac{1}{4^{r}} [\mathrm{Tr}(\widetilde{\mathbf{A}}^{\mathrm{T}}\widetilde{\mathbf{A}})]^{\tau} ||\mathbf{X}_{L} - \mathbf{X}_{U}||^{2} + (\epsilon_{c} - \epsilon_{c}^{2}) \mathrm{Tr}(\mathbf{K}^{\mathrm{T}}\widetilde{\mathbf{B}}^{\mathrm{T}}\widetilde{\mathbf{B}}\mathbf{K}) \mathbf{X}_{M}^{\mathrm{T}} \mathbf{X}_{M} \frac{1 - [\mathrm{Tr}(\widetilde{\mathbf{A}}^{\mathrm{T}}\widetilde{\mathbf{A}})]^{\tau}}{1 - \mathrm{Tr}(\widetilde{\mathbf{A}}^{\mathrm{T}}\widetilde{\mathbf{A}})}.$$
(29)

And when $Tr(\widetilde{\mathbf{A}}^T\widetilde{\mathbf{A}}) = 1$,

$$\mathbb{E}[\mathbf{e}_{\tau}^{\mathrm{T}}\mathbf{e}_{\tau}] \leqslant \frac{1}{12} \frac{1}{4^{r}} [(\mathbf{X}_{L} - \mathbf{X}_{U})^{\mathrm{T}} (\mathbf{X}_{L} - \mathbf{X}_{U})] + (\epsilon_{c} - \epsilon_{c}^{2})\tau$$

$$\cdot \operatorname{Tr}(\mathbf{K}^{\mathrm{T}} \widetilde{\mathbf{B}}^{\mathrm{T}} \widetilde{\mathbf{B}} \mathbf{K}) \mathbf{X}_{M}^{\mathrm{T}} \mathbf{X}_{M},$$
(30)

where $\mathbf{X}_{M} = \{x_{M,i} | x_{M,i} = \max\{|x_{U,i}|, |x_{L,i}|\}\}$, with $x_{U,i}$ and $x_{L,i}$ being the *i*th element of matrix \mathbf{X}_{U} and \mathbf{X}_{L} , respectively, where $i \in \{1, 2, ..., n\}$. The proofs of (29) and (30) are provided in Appendix D. According to (29) and (30), a common bound for any τ with the delay bound $D_{c,\max}$ can be obtained as

$$\mathbb{E}[\mathbf{e}_{ au}^{\mathrm{T}}\mathbf{e}_{ au}]$$

$$\leqslant \begin{cases}
\frac{1}{12} \frac{1}{4^{r}} [\operatorname{Tr}(\widetilde{\mathbf{A}}^{T} \widetilde{\mathbf{A}})]^{\lfloor D_{c,\max}/T_{d} \rfloor} [(\mathbf{X}_{L} - \mathbf{X}_{U})^{T} (\mathbf{X}_{L} - \mathbf{X}_{U})], \\
+ (\epsilon_{c} - \epsilon_{c}^{2}) \operatorname{Tr}(\mathbf{K}^{T} \widetilde{\mathbf{B}}^{T} \widetilde{\mathbf{B}} \mathbf{K}) \mathbf{X}_{M}^{T} \mathbf{X}_{M} \frac{1 - [\operatorname{Tr}(\widetilde{\mathbf{A}}^{T} \widetilde{\mathbf{A}})]^{\lfloor D_{c,\max}/T_{d} \rfloor}}{1 - \operatorname{Tr}(\widetilde{\mathbf{A}}^{T} \widetilde{\mathbf{A}})}, \text{ when } \operatorname{Tr}(\widetilde{\mathbf{A}}^{T} \widetilde{\mathbf{A}}) > 1, \\
\frac{1}{12} \frac{1}{4^{r}} [(\mathbf{X}_{L} - \mathbf{X}_{U})^{T} (\mathbf{X}_{L} - \mathbf{X}_{U})] + (\epsilon_{c} - \epsilon_{c}^{2}) \frac{\operatorname{Tr}(\mathbf{K}^{T} \widetilde{\mathbf{B}}^{T} \widetilde{\mathbf{B}} \mathbf{K}) \mathbf{X}_{M}^{T} \mathbf{X}_{M}}{1 - \operatorname{Tr}(\widetilde{\mathbf{A}}^{T} \widetilde{\mathbf{A}})}, \text{ when } \operatorname{Tr}(\widetilde{\mathbf{A}}^{T} \widetilde{\mathbf{A}}) < 1, \\
\frac{1}{12} \frac{1}{4^{r}} [(\mathbf{X}_{L} - \mathbf{X}_{U})^{T} (\mathbf{X}_{L} - \mathbf{X}_{U})] + (\epsilon_{c} - \epsilon_{c}^{2}) \lfloor D_{c,\max}/T_{d} \rfloor \cdot \operatorname{Tr}(\mathbf{K}^{T} \widetilde{\mathbf{B}}^{T} \widetilde{\mathbf{B}} \mathbf{K}) \mathbf{X}_{M}^{T} \mathbf{X}_{M}, \text{ when } \operatorname{Tr}(\widetilde{\mathbf{A}}^{T} \widetilde{\mathbf{A}}) = 1
\end{cases}$$

$$\dot{=} F_{e}(r, \epsilon_{c}, D_{c,\max}). \tag{31}$$

2.4 Convergence analysis of the closed-loop system

To quantitatively analyze the impact of communication, sensing, and estimation on the performance of control systems, this section introduces an analytical framework based on the Lyapunov theory. Through this framework, we next derive inequalities that establish a relationship between the system's convergence rate and key factors such as delay, packet loss, and estimation errors.

According to the LaSalle's invariance principle [15, 39], the system converges at a rate of ρ , if

$$\mathbb{E}\left[V_f(\mathbf{X}_{t+1})|\mathbf{X}_t\right] \leqslant \rho V_f(\mathbf{X}_t),\tag{32}$$

where $V_f(\cdot)$ is the Lyapunov function of the closed-loop system, which is defined as [40, Ch. 4.2]

$$V_f(\mathbf{X}_t) = \mathbf{X}_t^T \mathbf{P} \mathbf{X}_t \doteq |\mathbf{X}_t|_{\mathbf{P}}^2 \tag{33}$$

with \mathbf{P} being a pre-defined semi-positive definite matrix.

Based on (20), (32), and (33), the impact of communication and sensing on the convergence of the closed-loop system is derived in Theorem 4.

Theorem 4 (Convergence rate inequality). The sufficient condition of the system convergence (32) is satisfied if

$$\rho \geqslant \frac{F_{\rho}(W_u, W_d, \mathbf{K}, \mathbf{X}_t)}{|\mathbf{X}_t|_{\mathbf{P}}^2},\tag{34}$$

where

$$F_{\rho}(W_{u}, W_{d}, \mathbf{K}, \mathbf{X}_{t}) = (1 - \epsilon_{c})\{-|\widetilde{\mathbf{A}}\mathbf{X}_{t}|_{\mathbf{P}}^{2} + |(\widetilde{\mathbf{A}} + \widetilde{\mathbf{B}}\mathbf{K})\mathbf{X}_{t}|_{P}^{2} + F_{e}(r, \epsilon_{c}, D_{c, \max}) \text{Tr}[|\mathbf{B}\mathbf{K}|_{\mathbf{P}}^{2}]\} + |\widetilde{\mathbf{A}}\mathbf{X}_{t}|_{\mathbf{P}}^{2},$$
(35)

and $F_e(r, \epsilon_c, D_{c,\text{max}})$ is given in (31).

Proof. See the proof in Appendix E.

The closed-form inequality in (34) quantitatively characterizes how the convergence rate of the closed-loop system depends on key parameters. This result provides explicit guidance for resource allocation and parameter configuration, serving as a sufficient condition for system convergence, and can therefore be regarded as a conservative design criterion. Despite its conservative nature, this closed-form expression remains a practical tool for evaluating and optimizing the joint effects of communication, sensing, and control parameters.

3 Optimization of control strategy and resource allocation

As illustrated in Figure 3, to ensure the on-demand equipment operations, it is essential to design the optimal control law, i.e., **K**. However, as can be inferred from the system model, the performance of communication, sensing, and control is intricately linked. Therefore, to achieve the control objectives, it is necessary to simultaneously regulate the resources such as the bandwidth, quantization levels, and control strategies. Considering the complexity of such a problem, a constrained model predictive control (MPC) strategy is applied to simultaneously generate the optimal control law and the resource allocation strategy [40].

$$J(\mathbf{K}, W_u, W_d) = \sum_{t=0}^{N-1} \left[\hat{\mathbf{X}}_t^{\mathrm{T}} \mathbf{Q} \hat{\mathbf{X}}_t + (\mathbf{K} \hat{\mathbf{X}}_t)^{\mathrm{T}} \mathbf{R} (\mathbf{K} \hat{\mathbf{X}}_t) \right] + \frac{1}{2} \hat{\mathbf{X}}_N^{\mathrm{T}} \mathbf{P}_f \hat{\mathbf{X}}_N,$$
(36)

where N is the prediction horizon in which the future states are considered. The term $\hat{\mathbf{X}}_t^T \mathbf{Q} \hat{\mathbf{X}}_t$, which can be reformed as $(\hat{\mathbf{X}}_t - \mathbf{0})^T \mathbf{Q} (\hat{\mathbf{X}}_t - \mathbf{0})$, is the distances between $\hat{\mathbf{X}}_t$ and the control objective $\hat{\mathbf{X}} = \mathbf{0}$ at time t. $(\mathbf{K}\hat{\mathbf{X}}_t)^T \mathbf{R} (\mathbf{K}\hat{\mathbf{X}}_t)$ represents the amount of energy expended during the control process. Both \mathbf{Q} and \mathbf{R} are predetermined positive semi-definite matrices that respectively reflect the weighted relationships between state changes and control energy, with their values carefully chosen to meet practical requirements. The summation term represents the total control cost over the next N time instants. $\frac{1}{2}\hat{\mathbf{X}}_N^T \mathbf{P}_f \hat{\mathbf{X}}_N$ is the terminal cost [40], the purpose of which is to compensate for the control cost, bringing it closer to the result when $N = \infty$, so as to enhance the control performance. \mathbf{P}_f is the solution of the discrete Racciti function [40, Ch. 2.5], given by

$$\mathbf{P}_{f} = \mathbf{Q} + \widetilde{\mathbf{A}}^{\mathrm{T}} \mathbf{P}_{f} \widetilde{\mathbf{A}} - \widetilde{\mathbf{A}}^{\mathrm{T}} \mathbf{P}_{f} \widetilde{\mathbf{B}} \left(\mathbf{R} + \widetilde{\mathbf{B}}^{\mathrm{T}} \mathbf{P}_{f} \widetilde{\mathbf{B}} \right)^{-1} \widetilde{\mathbf{B}}^{\mathrm{T}} \mathbf{P}_{f} \widetilde{\mathbf{A}}. \tag{37}$$

According to Theorems 3 and 4, the state function (20), and the bandwidth limit, the optimization problem is formulated as

P1:
$$\min_{\mathbf{K}, W_u, W_d} J(\mathbf{K}, W_u, W_d),$$
 (38a)

s.t.
$$\lambda_u \leqslant \lambda_{\max}$$
, (38b)

$$\rho \geqslant \frac{F_{\rho}(W_u, W_d, \mathbf{K}, \hat{\mathbf{X}}_t)}{|\hat{\mathbf{X}}_t|_{\mathbf{P}}^2},\tag{38c}$$

$$0 \leqslant W_u + W_d \leqslant W_0, \tag{38d}$$

$$0 \leqslant \epsilon_c \leqslant 1,$$
 (38e)

$$\hat{\mathbf{X}}_{t+1} = \mathbf{A}_K \hat{\mathbf{X}}_t. \tag{38f}$$

In the above optimization problem, constraints (38b) and (38c) are the solutions of Theorems 3 and 4, respectively. Constraint (38d) constraints the available bandwidth of the communication. Constraint (38e) guarantees the correct range of packet loss rate. Constraint (38f) is the estimation rule in (26).

Due to the complex structure of constraint (38c), this optimization problem is non-convex. The DE method is particularly effective for this kind of non-convex problems due to its robust global search capability, which significantly enhances the probability of finding the global optimum. Therefore, DE-based optimization method is employed to seek the global optimal solution for this problem [41,42], as Algorithm 1.

4 Simulation results

In this section, the motion control of an AGV is simulated to demonstrate the effectiveness of the proposed control strategy and resource allocation method. Furthermore, we conduct an analysis to investigate the dynamic influence of parameter variations on the system. For each experiment, 500 times of Monte-Carlo trials are conducted to ensure statistical reliability. The setting of the parameters is shown in Table 1.

The iteration of the system is carried out based on the delay-compensation control method proposed in Subsection 2.2, as shown in Figure 3. The performance of the system is evaluated by three time-varying indicators, i.e., state distance, accumulated control energy, and accumulated cost. The definitions of the three indicators are provided in the sequel.

Algorithm 1 DE-based optimization method.

Input: System parameters such as W_0 , θ_u , θ_d , SNR_u , and SNR_d . Algorithm parameters such as population size N_p , crossover probability p_{cr} , differential weight F_d , maximum iterations N_m , maximum counter n, and tolerance of convergence tol1: Solve \mathbf{P}_f according to (37); 2: Randomly initialize population with N_p individuals; 3: Initialize best fitness change counter: counter = 0; 4: for i = 1 to N_m and counter < n do for each individual $\mathbf{\Xi}_k = [K_k, W_{u,k}, W_{d,k}]$ do Randomly select three individuals Ξ_{r1} , Ξ_{r2} , Ξ_{r3} from the population; 6: 7: Compute the mutant vector: $\mathbf{V}_k = \mathbf{\Xi}_{r1} + F_d \times (\mathbf{\Xi}_{r2} - \mathbf{\Xi}_{r3});$ Let $\mathbf{H}_k = \mathbf{V}_k$ with probability p_{cr} and $\mathbf{H}_k = \mathbf{\Xi}_i$ with probability $1 - p_{cr}$; 8: if {Constraints are not violated for \mathbf{U}_k and $J(\mathbf{U}_k) < J(\mathbf{\Xi}_k)$ } or Constraints are violated for $\mathbf{\Xi}_k$ then 9. 10: Replace Ξ_k with U_k in the population; end if 11: 12: end for 13: if $|\min J(\mathbf{H}_k) - \min J(\mathbf{\Xi}_k)| < tol$ then 14: Increment counter by 1; 16: Reset counter to 0; 17: end if 18: end for 19: Output: The individual corresponding to the Fitness_{current}.

Parameter	Value	Parameter	Value
	System p	parameters	
T_d	$0.1\mathrm{s}$	ς	0.125
P	diag(10, 10, 1)	Q	$\mathrm{diag}(10,10,1)$
R	1	\mathbf{X}_0	$[-100, 1, 1]^{\mathrm{T}}$
N	10	c_d	0.1
SNR_u	$30\mathrm{dB}$	SNR_d	$33\mathrm{dB}$
eta_u	1	eta_d	1
θ_u	0.02	$ heta_d$	0.04
W_0	$1.5\mathrm{MHz}$		
	Algorithm	parameters	
N_p	15	p_{cr}	0.7
n	5	N_m	1000
tol	0.01	F_d	0.5

Table 1 Simulation parameters

• The state distance is the quadratic form of the state \mathbf{X}_t , which reveals the distance from state \mathbf{X}_t to state $\mathbf{0}$, i.e.,

$$SD = \mathbf{X}_t^{\mathrm{T}} \mathbf{Q} \mathbf{X}_t, \tag{39}$$

where SD represents the state distance.

• The accumulated control energy is the total of control energy from the initial time to the current time, i.e.,

$$ACE = \sum_{t=0}^{N-1} \left[(\mathbf{K} \mathbf{X}_t)^{\mathrm{T}} \mathbf{R} (\mathbf{K} \mathbf{X}_t) \right], \tag{40}$$

where ACE represents the accumulated control energy.

• The accumulated cost is the total control cost from the initial time to the current, which is the sum part of (36), i.e.,

$$AC = \sum_{t=0}^{N-1} \left[\mathbf{X}_t^{\mathrm{T}} \mathbf{Q} \mathbf{X}_t + (\mathbf{K} \mathbf{X}_t)^{\mathrm{T}} \mathbf{R} (\mathbf{K} \mathbf{X}_t) \right], \tag{41}$$

where AC represents the accumulated cost.

4.1 Impact of closed-loop delay

The impact of closed-loop delay $D_{c,\text{max}}$ on the system is shown in Figure 4, where $D_{c,\text{max}}$ varies from 0.06 to 0.1 s, $\rho = 0.999$, and r = 6. As illustrated in Figure 4(a), it can be observed that the convergence speed of states significantly increases with the reduction of the maximum allowable closed-loop delay, which is due to the fact

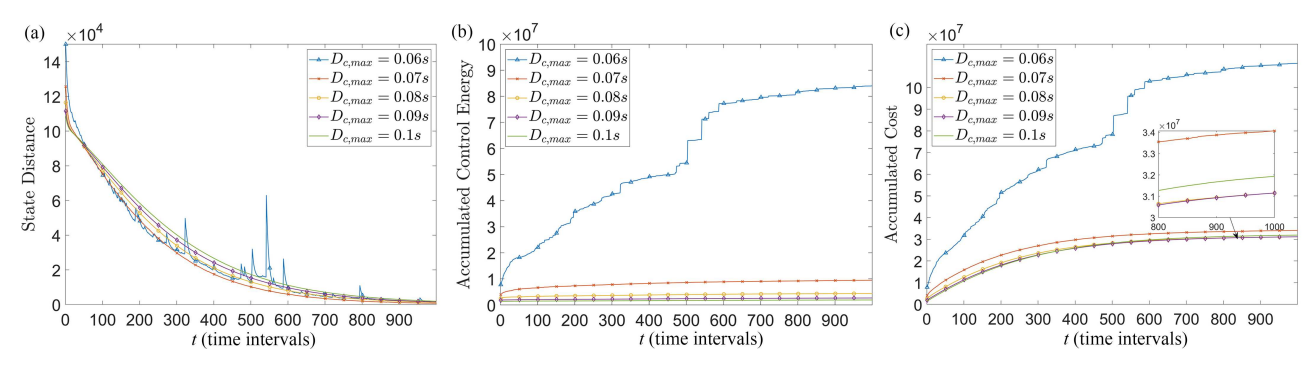


Figure 4 (Color online) Variations of (a) state distance, (b) accumulated control energy, and (c) accumulated cost with closed-loop delay constraints.

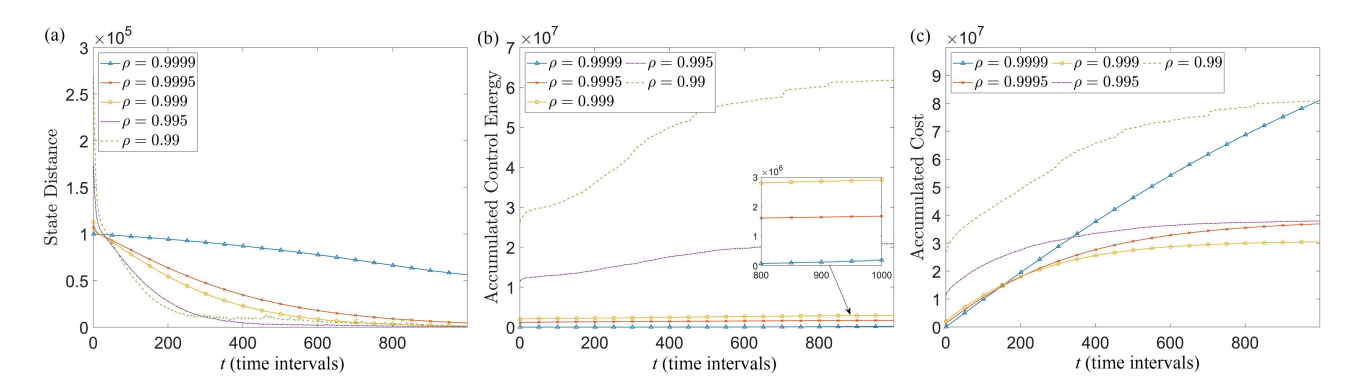


Figure 5 (Color online) Variations of (a) state distance, (b) accumulated control energy, and (c) accumulated cost with different convergence rates.

that strict delay constraints enhance the timeliness of control commands. However, when $D_{c,\text{max}}$ is too small, such as $D_{c,\text{max}} = 0.06\,\text{s}$ in Figure 4(a), the system experiences a high packet loss rate due to (8). This leads to the failure of most control commands in reaching the actuators, consequently resulting in significant fluctuations in the device's state. For the same reason, Figure 4(b) demonstrates that excessively strict constraints on delay, i.e., $D_{c,\text{max}} = 0.06\,\text{s}$, significantly augment the consumption of control energy. Furthermore, increasing $D_{c,\text{max}}$ reduces the packet loss rate, diminishing the need for large control actions against packet loss impacts. Consequently, the accumulated control energy gradually decreases.

From Figures 4(a) and (b), it can be observed that although an increase in $D_{c,\text{max}}$ leads to a reduction in control energy consumption, it also results in a slower convergence. This results in a reduction of the accumulated cost with the increase of $D_{c,\text{max}}$ during the early stages of the control process, i.e., when $t \leq 500$. Conversely, when $t \geq 500$, within the interval where $D_{c,\text{max}} \geq 0.08 \, \text{s}$, the accumulated cost increases with the rise of $D_{c,\text{max}}$. This is because although a higher $D_{c,\text{max}}$ entails lower accumulated control energy consumption, its slower convergence leads to a longer accumulation period for control costs. Over time, this results in a higher accumulated cost.

4.2 Impact of convergence rate

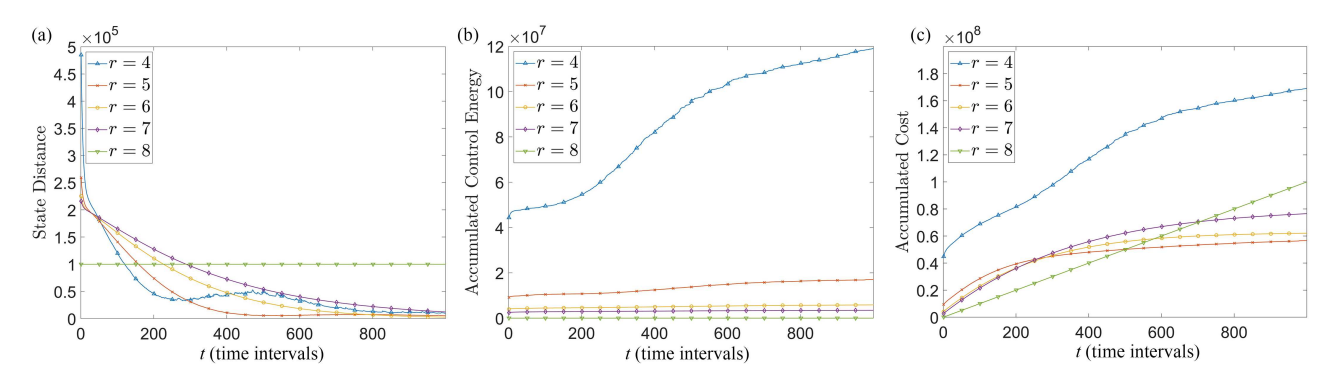


Figure 6 (Color online) Variations of (a) state distance, (b) accumulated control energy, and (c) accumulated cost with different quantization levels.

4.3 Impact of quantization level

The impact of quantization level r on the system is shown in Figure 6, where r varies from 4 to 8, $D_{c,\text{max}} = 0.1 \,\text{s}$, and $\rho = 0.999$. It is evident that when the value of r is sufficiently small, particularly when r = 4, the convergence of the system is hindered, leading to a substantial increase in both accumulated cost and control energy. This is because the estimation error is much too large, making it difficult for the control instructions to accurately identify the current state. Furthermore, an excessively large r, such as r = 8 as depicted in the figure, leads to an unsolvable optimization problem. This situation obstructs the generation of control commands by the control center, thus limiting the actuator's capacity to achieve convergence.

Except for the above situations, a larger r results in a faster convergence and smaller control energy, as r respectively equals 5, 6, and 7 in Figures 6(a) and (b). In such cases, a decrease in quantization level leads to an increase in sensing errors, subsequently requiring higher control energy from the device to sustain control operations. Ultimately, this contributes to increased control power consumption. However, increasing the quantization order places a heavier burden on the communication link, resulting in an increased average time delay and slower convergence. Furthermore, the accumulated cost is the combination of the state distance and the accumulated control energy. Despite the higher initial control energy consumption associated with a smaller quantization level before t = 250, a faster convergence rate is achieved for smaller r when $r \ge 5$ and $t \ge 250$, which results in a lower accumulated cost overall, as demonstrated in Figure 6(c).

5 Conclusion

The existing theoretical models for closed-loop control systems with wireless networks fail to achieve the expected control effects in practical applications, thus resulting in challenges in the design of communication, sensing, and control systems. To address the issue of the separation between uplink and downlink models, an uplink-downlink coupled closed-loop communication model was first proposed based on the transmission characteristics of the industrial wireless networks. The closed-form expressions of closed-loop delay and packet loss rate were next derived to provide more practical metrics for the industrial system. Subsequently, a control model based on the delay compensation algorithm and packet loss was presented, as well as a sensing-estimation model based on quantization and estimation error. In order to model the relationship between communication, sensing, and control, the inequality related to communication, sensing, and control parameters was derived based on the proposed models. The result provided a lower bound on the convergence rate that ensures system stability. Finally, to provide guidance for the design of the closed-loop system, a joint optimization problem for control and resource allocation was introduced. An algorithm based on DE was presented to obtain the global optimal solution of the non-convex problem. Numerical simulations indicated that due to the interdependencies among communication, sensing, and control systems, excessively high or low parameter designs can markedly degrade the system's control effectiveness.

6 Future work

This work establishes an integrated framework for closed-loop control systems, focusing on the interplay among sensing, communication, and control under periodic, single-sensor operation. To further enhance both the theoretical

richness and the practical relevance of the proposed model, several promising directions can be considered in future research.

One important direction is to generalize the proposed framework to accommodate non-periodic or event-driven data transmission schemes. While the periodic sampling and reporting assumption align with current industrial standards and is widely adopted in mainstream deployments, there are scenarios, such as event-triggered or application-adaptive reporting, where sensor transmissions become non-periodic. Extending the analysis and optimization framework to such cases, and investigating how time-varying traffic patterns and communication delays influence closed-loop system stability and control performance, will further broaden the applicability of integrated sensing-communication-control models to a wider range of practical industrial environments.

A further promising avenue is to extend the framework to integrated sensing and communication (ISAC) technologies [19, 20, 43–48]. ISAC allows wireless networks to simultaneously support communication and sensing, unifying these functions at the physical and protocol layers. This integration can fundamentally change traditional closed-loop processes by reducing or even eliminating the separate sensing time of conventional sensors, potentially leading to significant latency improvements. Future research can focus on joint modeling and optimization of ISAC-enabled systems, investigating how real-time scene information, joint waveform design, and co-optimized resource allocation affect the stability and performance of closed-loop control. Exploring these aspects will provide valuable insights for next-generation industrial systems with enhanced efficiency and responsiveness.

It is also valuable to generalize the current framework to multi-sensor systems. When multiple sensors observe the same target, the system architecture can be viewed as a set of parallel sensing-communication links. This redundancy not only improves reliability and robustness against data loss, but also introduces new challenges in communication resource allocation and scheduling. From an information-theoretic perspective, the scenario in which each sensor acquires a noisy observation and independently transmits quantized data to a central processor can be viewed as a typical multi-terminal source coding problem, where the fusion center reconstructs the underlying state based on all received data. The overall performance then depends on the joint effects of all communication links, sensor errors, and the data fusion algorithm. Extending the integrated model to this scenario will involve joint modeling of multi-source sensing, multi-channel communication, and data fusion, as well as investigating their influence on closed-loop control stability and performance.

These extensions will provide valuable theoretical insights and design guidelines for practical industrial closed-loop control systems with more diverse and complex architectures.

Acknowledgements This work was supported in part by National Natural Science Foundation of China (Grant Nos. U21B2014, 92267202), Fundamental Research Funds for the Central Universities (Grant No. 2024ZCJH01), and National Key Research and Development Program of China (Grant No. 2020YFA0711303).

Supporting information Appendixes A–E. The supporting information is available online at info.scichina.com and link.springer.com. The supporting materials are published as submitted, without typesetting or editing. The responsibility for scientific accuracy and content remains entirely with the authors.

References

- 1 3GPP. Service requirements for the 5G System. TS 22.261 V19.1.0, 2022. https://portal.3gpp.org/desktopmodules/Specifications/SpecificationDetails.aspx?specificationId=3107
- 2 Huawei. 6G: the next horizon. Whitepaper. 2022. https://www-file.huawei.com/-/media/corp2020/pdf/tech-insights/1/6g-white-paper-en.pdf?la=en
- Rao S K, Prasad R. Impact of 5G technologies on industry 4.0. Wireless Pers Commun, 2018, 100: 145–159
- 4 Attaran M. The impact of 5G on the evolution of intelligent automation and industry digitization. J Ambient Intell Hum Comput, 2023, 14: 5977-5993
- 5 Meng Z, Ma D, Wang S, et al. Modeling and design of the communication sensing and control coupled closed-loop industrial system. In: Proceedings of 2023 IEEE Global Communications Conference, 2023
- 6 Krstic M, Smyshlyaev A. Backstepping boundary control for first-order hyperbolic PDEs and application to systems with actuator and sensor delays. Syst Control Lett, 2008, 57: 750–758
- 7 Liu G P. Predictive controller design of networked systems with communication delays and data loss. IEEE Trans Circuits Syst II Express Briefs, 2010, 57: 481–485
- 8 Huang K, Liu W, Li Y, et al. Optimal downlink-uplink scheduling of wireless networked control for industrial IoT. IEEE Internet Things J, 2020, 7: 1756–1772
- 9 Zhang D W, Han Q-L, Jia X C. Network-based output tracking control for a class of T-S fuzzy systems that can not be stabilized by nondelayed output feedback controllers. IEEE Trans Cybern, 2014, 45: 1511–1524
- 10 Ayidh A A, Chang B, Zhao G, et al. Energy-efficient power allocation in URLLC enabled wireless control for factory automation applications. In: Proceedings of the IEEE 31st Annual International Symposium on Personal, Indoor and Mobile Radio Communications, London, 2020. 1–6
- 11 Borri A, Pola G, Benedetto M D D. Design of symbolic controllers for networked control systems. IEEE Trans Automat Contr, 2019, 64: 1034–1046
- 12 Schenato L, Sinopoli B, Franceschetti M, et al. Foundations of control and estimation over lossy networks. Proc IEEE, 2007, 95: 163-187
- 13 Kostina V, Hassibi B. Rate-cost tradeoffs in control. IEEE Trans Automat Contr, 2019, 64: 4525-4540
- 14 Yang H, Zhang K, Zheng K, et al. Leveraging linear quadratic regulator cost and energy consumption for ultrareliable and low-latency IoT control systems. IEEE Internet Things J, 2020, 7: 8356–8371
- 15 Gatsis K, Pajic M, Ribeiro A, et al. Opportunistic control over shared wireless channels. IEEE Trans Automat Contr, 2015, 60: 3140–3155

- 16 Chang B, Zhang L, Li L, et al. Optimizing resource allocation in URLLC for real-time wireless control systems. IEEE Trans Veh Technol, 2019, 68: 8916–8927
- 17 Chang B, Li L, Zhao G, et al. Autonomous D2D transmission scheme in URLLC for real-time wireless control systems. IEEE Trans Commun, 2021, 69: 5546–5558
- 18 Chang B, Tang W, Yan X, et al. Integrated scheduling of sensing, communication, and control for mmWave/THz communications in cellular connected UAV networks. IEEE J Sel Areas Commun, 2022, 40: 2103–2113
- 19 Bazzi A, Chafii M. Low dynamic range for RIS-aided bistatic integrated sensing and communication. IEEE J Sel Areas Commun, 2025, 43: 912-927
- 20 Bazzi A, Chafii M. Mutual information based pilot design for ISAC. IEEE Trans Commun, 2025, doi: 10.1109/TCOMM.2025.3545658
- 21 Pukdeboon C. A review of fundamentals of Lyapunov theory. J Appl Sci, 2011, 10: 55–61
- 22 Bilal, Pant M, Zaheer H, et al. Differential evolution: a review of more than two decades of research. Eng Appl Artif Intelligence, 2020, 90: 103479
- 23 Zhang X M, Han Q L, Ge X, et al. Networked control systems: a survey of trends and techniques. IEEE CAA J Autom Sin, 2020, 7: 1–17
- 24 Liu W, Nair G, Li Y, et al. On the latency, rate, and reliability tradeoff in wireless networked control systems for IIoT. IEEE Internet Things J, 2021, 8: 723–733
- 25 Lu Z, Guo G. Control and communication scheduling co-design for networked control systems: a survey. Int J Syst Sci, 2022, 54: 189-203
- 26 Zhang L, Wang C X, Zhou Z, et al. Wireless channel measurements and characterization in industrial IoT scenarios. IEEE Trans Veh Technol, 2025, 74: 2292–2307
- 27 Zavorka R, Mikulasek T, Vychodil J, et al. Long-term channel analysis at 60 and 80 GHz for autonomous ground vehicles. In: Proceedings of IEEE Conference on Antenna Measurements and Applications (CAMA), 2024. 1–6
- 28 Leemis L M. Rayleigh exponential theorem. College of William and Mary, 2012. https://www.math.wm.edu/~leemis/chart/UDR/PDFs/RayleighExponential.pdf
- 29 Wu D, Negi R. Effective capacity: a wireless link model for support of quality of service. IEEE Trans Wireless Commun, 2003, 2: 630-643
- 30 Khalek A A, Caramanis C, Heath R W. Delay-constrained video transmission: quality-driven resource allocation and scheduling. IEEE J Sel Top Signal Process, 2015, 9: 60–75
- 31 Bubnicki Z. Formal models of control systems. In: Modern Control Theory. Berlin: Springer, 2005. 17–37
- 32 Mei J, Zheng K, Zhao L, et al. Joint radio resource allocation and control for vehicle platooning in LTE-V2V network. IEEE Trans Veh Technol. 2018, 67: 12218–12230
- 33 Iqbal J. Modern control laws for an articulated robotic arm: modeling and simulation. Eng Technol Appl Sci Res, 2019, 9: 4057-4061
- 34 Galias Z, Yu X. Euler's discretization of single input sliding-mode control systems. IEEE Trans Automat Contr, 2007, 52: 1726-1730
- 35 Goulart P J, Kerrigan E C, Maciejowski J M. Optimization over state feedback policies for robust control with constraints. Automatica, 2006, 42: 523–533
- 36 Teng L, Wang Y, Cai W, et al. Fuzzy model predictive control of discrete-time systems with time-varying delay and disturbances. IEEE Trans Fuzzy Syst, 2018, 26: 1192–1206
- 37 Chang B, Yan X, Zhang L, et al. Joint communication and control for mmWave/THz beam alignment in V2X networks. IEEE Internet Things J, 2022, 9: 11203-11213
- 38 Liu G P, Mu J X, Rees D, et al. Design and stability analysis of networked control systems with random communication time delay using the modified MPC. Int J Control, 2006, 79: 288–297
- 39 Sastry S. Lyapunov stability theory. In: Nonlinear Systems: Analysis, Stability, and Control. Berlin: Springer, 1999. 182–234
- 40 JBJ B R, Mayne D Q. Model Predictive Control Theory and Design. Santa Barbara: Nob Hill Publishing, LLC, 1999
- 41 Ahmad M F, Isa N A M, Lim W H, et al. Differential evolution: a recent review based on state-of-the-art works. Alexandria Eng J, 2022, 61: 3831–3872
- 42 Parouha R P, Verma P. A systematic overview of developments in differential evolution and particle swarm optimization with their advanced suggestion. Appl Intell, 2022, 52: 10448–10492
- 43 Yu Z, Ren H, Pan C, et al. Addressing the mutual interference in uplink ISAC receivers: a projection method. IEEE Wireless Commun Lett, 2024, 13: 3109–3113
- 44 Yu Z, Ren H, Pan C, et al. A framework for uplink ISAC receiver designs: performance analysis and algorithm development. 2025. ArXiv:2503.02647
- 45 Zhang J F, Lu W D, Xing C W, et al. Intelligent integrated sensing and communication: a survey. Sci China Inf Sci, 2025, 68: 131301
- 46 Xiao Y, Wang E H, Chen Y F, et al. Communication-centric integrated sensing and communications with mixed fields. Sci China Inf Sci, 2024, 67: 219301
- 47 Liu G Y, Xi R Y, Jiang T, et al. Feasibility study of cooperative sensing: radar cross section, synchronization, cooperative cluster, performance and prototype. Sci China Inf Sci, 2025, 68: 150302
- 48 Song X X, Fang Y, Wang F, et al. An overview on IRS-enabled sensing and communications for 6G: architectures, fundamental limits, and joint beamforming designs. Sci China Inf Sci, 2025, 68: 150301